2024 5th International Conference on Computer, Big Data and Artificial Intelligence (ICCBD+AI) | 979-8-3315-3399-1/24/$31.00 ©2024 IEEE | DOI: 10.1109/ICCBD-AI65562.2024.00033

Towards Image Denoising via Random Interpolation and Hard Thresholding

1st Jinhao Lin
Future Technology
South China University of Technology
Guangzhou, China
ftlinjinhao@mail.scut.edu.cn

2nd Qiwei Xiong
Electronic and Information Engineering
South China University of Technology
Guangzhou, China
xiongqiwei@vip.qq.com

3rd Yuxiao Wang
Future Technology
South China University of Technology
Guangzhou, China
ftwangyuxiao@mail.scut.edu.cn

4th Weiying Xue
Future Technology
South China University of Technology
Guangzhou, China
202320163283@mail.scut.edu.cn

5th Qi Liu
Future Technology
South China University of Technology
Guangzhou, China
drliuqi@scut.edu.cn

6th Zhenao Wei*
Future Technology
South China University of Technology
Guangzhou, China
wza@scut.edu.cn

***Abstract*—Image denoising refers to producing a crystal clear digital image from a noisy capture environment since the natural image is inevitably contaminated during phases of acquisition and transmission by different kinds of noises, such as salt and pepper noise (SAPN) and additive white Gaussian noise (AWGN). Towards the mixed noise removal, it is well known that the least squares-based metric is highly sensitive to outliers, and one common practice is using ℓ_p-norm minimization to restore the noise-free image. However, the resulting minimization problem is challenging to guarantee its convergence because of the nonconvexity of ℓ_p-norm. Moreover, its performance is greatly affected by the choice of p. On the basis of that, we propose to employ low-rank matrix factorization to form the basic denoising framework due to the advantage of preserving the spatial integrity of the image. Herein, the noisy image is randomly sampled to produce sampled image sets to mitigate the SPAN. An alternating minimization method is applied to all sampled images and the resultant images are fused via a wavelet fusion with hard threshold denoising. Since the sampled image sets have independent but identical noise property, the wavelet fusion serves as the effective means to remove the AWGN. Simulation results are presented vividly to show the impressive performance in both subjective and objective metrics.**

***Index Terms*—Image denoising, mixed noise removal, low-rank matrix factorization, 2-D random interpolation averaging.**

I. Introduction

As a fundamental and important problem for image processing and computer vision, image denoising has caught increasing attention in past few years. It is because the natural image is inevitably contaminated by noise during phases of acquisition and transmission, which is the major source of noise degrading the image quality in the subsequent image processing applications, including edge detection, object segmentation and feature extraction [1]–[3].

Many techniques have been proposed to perform image denoising, e.g., spatial domain-based method [4], statistical modeling based method [5], order statistics method [6], and transform domain-based methods [7]–[11]. The transform domain methods are popular in literature because of their effectiveness in reducing the complexity of the image representation, where they first transform the spatial domain image into transform domain image.

In [9], although the split augmented Lagrangian shrinkage algorithm (SALSA) applied in small noise image has achieved good performance and faster computation, its result is unsatisfactory especially in strong additive white Gaussian noise (AWGN). Moreover, its performance is often limited by the sparsifying capacity of the transform, such that the more sparse the representation, the better the denoising result. Some sparse denoising methods need to decompose the noisy image into several blocks (patches) first, and then perform sparse representation for each small block under certain fixed atom library, the resultant sparsity optimization problem with dictionary learning is still computationally demanding [7]. In addition, some need to know the noise variance to normalize the F-norm data fidelity term so as to denoise the image, which is not practical since it may be hard to detect the noise variance especially in the case of the mixed noise.

Another class of the image denoising scheme is the spatial domain technique, which directly tackles the intensity of each pixel of the image, such as bilateral filter [12] and non-local means (NLM) filter [4], [13]. Due to the limitation of bilateral filter in preserving gradient direction of edges, NLM filter has been considered to have improved the overall denoising performance. Recently, the emerging technique of low-rank matrix factorization (LRMF) has given renewed interest to image denoising, and has a wide range of applications in computer vision. In weighted nuclear norm minimization (WNNM) algorithm [14], the low-rank regularization is enforced to reconstruct the latent structure of the noisy patch matrix. However, it only considers the non-local self-similarity property of the noise corrupted image, which makes it difficult to denoise the image from the noisy observation alone. In [15], a new hierarchical Bayesian generative model for the ℓ_1-norm LRMF problem is constructed to suppress the adverse

979-8-3315-3399-1/24/$31.00 ©2024 IEEE
DOI 10.1109/ICCBD-AI65562.2024.00033

influence of noises and outliers.

In this work, we propose a new image denoising method to tackle both salt-and-pepper noise (SAPN) and AWGN, which takes full advantages of the two-dimensional version of the random interpolation averaging (2-D RIA) method with good performance and robustness against impulsive noise. The LRMF method via alternating minimization is applied to the 2-D RIA generated image set. The processed images are fused together via wavelet fusion with hard threshold denoising to alleviate the AWGN in the resulting image set.

II. Problem Statement

We consider the image denoising problem from two major noise sources that affect the quality of digital images, namely, the AWGN due to random noise nature of image capturing devices and the SAPN due to hot pixels caused by current leakage in CMOS image sensors. Suppose that the original image $\mathbf{X} \in \mathbb{R}^{M\times N}$ is corrupted with mixed AWGN and SAPN, leading to the noisy image $\mathbf{M} \in \mathbb{R}^{M\times N}$. Without loss of generality, the AWGN and SAPN are assumed independent, such that the realistic model is written as [16], [17]:

$$\mathbf{Y} = \mathbf{X} + \mathbf{N},\ \mathbf{M} = Q(\mathbf{Y} \odot \mathbf{S}) \tag{1}$$

where $\mathbf{N}[i,j] \in \mathbb{Z}$ is the zero-mean AWGN, $\odot$ denotes the Hadamard multiplication, and the quantizer Q is defined as:

$$Q(x) = \begin{cases} x & 0 \le x \le \max \\ \max & x > \max \\ 0 & x \le 0 \end{cases} \tag{2}$$

and $\mathbf{S}$ is:

$$\mathbf{S}[i,j] = \begin{cases} \max - \mathbf{Y}[i,j] & \text{with probability } p_1 \\ -\mathbf{Y}[i,j] & \text{with probability } p_2 \\ \mathbf{Y}[i,j] & \text{with probability } 1-p_1-p_2. \end{cases} \tag{3}$$

$\mathbf{S}[i,j] \in [-\max, \max]$ denotes the (approximately) sparse matrix composed in the set of integer of SAPN which takes value as either the maximum available pixel brightness max (the salt) or the negative of it, such that the final pixel value equals 0 (the pepper). For gray-level image with 8 bits per pixel, the dynamic range of the pixel is $[0, 255]$ with $\max = 255$. Actually, the quantizer also acts as SAPN which takes their values in the dynamic range $[0, 255]$, known as the random-valued noise [16], [17].

III. The Proposed Method

Under the assumption of low-rankness[1], the mixed noise removal problem can be formulated as the following optimization problem via LRMF to approximately model $\mathbf{X}$, that is:

$$\min_{\mathbf{A},\mathbf{B}} \|(\mathbf{AB}) - \mathbf{M}\|_F^2, \tag{4}$$

where $\mathbf{A} \in \mathbb{R}^{M\times r}$ and $\mathbf{B} \in \mathbb{R}^{r\times N}$ with $r \ll \min\{M, N\}$, and $\|\cdot\|_F$ denotes the Frobenius norm. The intuition of using LRMF is avoiding to perform computationally demanding singular value decomposition (SVD) at each iteration and to choose the optimal regularizers as regularization-based models.

In general, the existing denoising works address the SAPN problem with ℓ_p-norm[2] minimization of the error term, where they design the denoising algorithms using ℓ_p-norm to restore the noise-free image from the noisy measurements. However, some of them cannot guarantee convergence due to the non-convexity of the resulting problem with highly nonconvex ℓ_p-norm. Moreover, the denoising performance of them are greatly affected by the choice of p. It is well known that least squares-based metric is highly sensitive to outliers present in the measurement vectors, leading to poor recovery.

The reasons using Frobenius norm data fitting model in (4) are included as follows. First, the goal of LRMA exploited in (4) is not for the SAPN reduction, instead of the randomly sampled image reconstruction for 2-D RIA. Any reconstruction method from randomly sampled image can be applied, and the use of Frobenius norm minimization is due to its convexity. Thereby, it is easier to find the closed-form solution based on the resultant least squares problem. Second, the idea of the proposed scheme is to utilize the random sampling and multiple images averaging to denoise SAPN, where the better denoisng performance from the following simulation results also implies that the reasonability of using Frobenius norm. The reason of better denoising performance is that the implemented method does not rely on the use of straight eigen-image, thus it provides relaxation to preserve complex image features when compared to that using few eigen-images alone to approximate the original image. Finally, the AWGN is being removed by averaging multiple SAPN removed images and we implement the averaging is a way that perform wavelet denoising to ensure the best reduction of AWGN. Since the key on the removal of SAPN in the proposed scheme depends on the random sampling and multiple image averaging, the use of Frobenius norm or ℓ_p-norm formulations would affect the denoising performance but it would not be critical.

Hence, we directly address (4) to reconstruct the random sampled images for 2-D RIA. For each random sampled image, (4) is converted to matrix Frobenius norm minimization:

$$\min_{\mathbf{A},\mathbf{B}} f(\mathbf{A},\mathbf{B}) \triangleq ||(\mathbf{AB}) - \mathbf{M}_\ell||_F^2, \ell = 1, \cdots, k \tag{5}$$

where $f(\mathbf{A},\mathbf{B})$ is defined as the error function, and k is the number of samples in two image sets. Unfortunately, the matrix Frobenius norm minimization problem in (5) with respect to (w.r.t.) $\mathbf{A}$ and $\mathbf{B}$ is nonconvex and is therefore

[1] A typical example in computer vision is Lambertian reflectance, where the vectors of $\mathbf{X}$ correspond to a set of images of a convex Lambertian surface under various lighting conditions [18]

[2] The ℓ_p-norm of a matrix denotes $||\mathbf{P}||_p = (\sum_{i,j} |P_{i,j}|^p)^{1/p}$

intractable. However, if we fix one of the two matrices, $\mathbf{A}$ or $\mathbf{B}$, $f(\mathbf{A},\mathbf{B})$ is convex w.r.t. the free matrix and the local/global minimum is readily available. As a result, an alternating minimization [19], [20] is applied to solve the resultant bi-convex optimization problem in (5). Consider $\mathbf{A}^t$ and $\mathbf{B}^t$ at the tth iteration, $\mathbf{A}^{t+1}$ and $\mathbf{B}^{t+1}$ are obtained sequentially by:

$$\min_{\mathbf{B}} f(\mathbf{B}^{t+1}) = ||(\mathbf{A}^t\mathbf{B}) - \mathbf{M}_\ell||_F^2, \tag{6}$$

$$\min_{\mathbf{A}} f(\mathbf{A}^{t+1}) = ||(\mathbf{A}\mathbf{B}^{t+1}) - \mathbf{M}_\ell||_F^2. \tag{7}$$

Both (6) and (7) are convex and obviously they have the same structure to be solved in a similar manner. Therefore, without loss of generality, we shall discuss the solver for $\mathbf{B}$, while the same method can be applied to $\mathbf{A}$ with straightforward modifications. Denote $\mathbf{A} = [\mathbf{a}_1, \cdots, \mathbf{a}_M]^T, \mathbf{B} = [\mathbf{b}_1, \cdots, \mathbf{b}_N]$, where the ith row of $\mathbf{A}$ and the jth column of $\mathbf{B}$ are represented as $\mathbf{a}_i^T \in \mathbb{R}^r, i = 1, ..., M$ and $\mathbf{b}_j \in \mathbb{R}^r, j = 1, ..., N$, respectively. For notational simplicity, the superscript $(\cdot)^t$ that denotes the iteration number is dropped in the following analysis without affecting the solution. To solve (6) for $\mathbf{B}$ with a fixed $\mathbf{A}$ [19], we rewrite (6) as:

$$\min_{\mathbf{b}_j} f(\mathbf{b}_j) = \sum_j |\mathbf{A}\mathbf{b}_j - \mathbf{m}_j|^2, \tag{8}$$

where $\mathbf{m}_j$ denotes the jth column of $\mathbf{M}_\ell$. Since $f(\mathbf{B})$ is decoupled w.r.t. $\mathbf{b}_j$, the solution for (8) can be obtained by finding the solutions of the following N independent sub-problems:

$$\min_{\mathbf{b}_j} f(\mathbf{b}_j) = ||\mathbf{A}\mathbf{b}_j - \mathbf{m}_j||_2^2, \tag{9}$$

which is a least squares problem, and its solution is $\mathbf{b}_j = \mathbf{A}^\dagger\mathbf{m}_j$. Similarly, the solution for (7) is $\mathbf{a}_i = (\mathbf{B}^T)^\dagger\mathbf{m}_i^T$, where $\mathbf{m}_i$ denotes the ith row of $\mathbf{M}_\ell$. After determining $\mathbf{A}$ and $\mathbf{B}$, the target matrix is obtained as $\hat{\mathbf{X}} = \mathbf{A}\mathbf{B}$.

Regarding the convergence, we first show that $||\mathbf{A}\mathbf{B} - \mathbf{M}_\ell||_F^2$ converges to a local minimum, and then extend our proof to show that $\{\mathbf{A},\mathbf{B}\}$ will also converge to a local optimum. Let the objective value $||\mathbf{A}\mathbf{B} - \mathbf{M}_\ell||_F^2$ after solving the two sub-problems in (6) and (7) be $E_{\mathbf{B}}^t$ and $E_{\mathbf{A}}^t$, respectively, at tth iteration. Since we have $E_{\mathbf{B}}^t = ||\mathbf{A}^{t-1}\mathbf{B}^t - \mathbf{M}_\ell||_F^2$ and $E_{\mathbf{A}}^t = ||\mathbf{A}^t\mathbf{B}^t - \mathbf{M}_\ell||_F^2$, the local optimality of $\mathbf{A}^t$ yields $E_{\mathbf{B}}^t \geq E_{\mathbf{A}}^t$. Similarly, at $(t+1)$-th iteration, $E_{\mathbf{A}}^t = ||\mathbf{A}^t\mathbf{B}^t - \mathbf{M}_\ell||_F^2$ and $E_{\mathbf{B}}^{t+1} = ||\mathbf{A}^t\mathbf{B}^{t+1} - \mathbf{M}_\ell||_F^2$, the local optimality of $\mathbf{B}^{t+1}$ yields $E_{\mathbf{A}}^t \geq E_{\mathbf{B}}^{t+1}$. Therefore, we get $E_{\mathbf{B}}^1 \geq E_{\mathbf{A}}^1 \geq E_{\mathbf{B}}^2 \geq \cdots \geq E_{\mathbf{B}}^t \geq E_{\mathbf{A}}^t \geq E_{\mathbf{B}}^{t+1} \geq \cdots$, that is, the objective value $||\mathbf{A}\mathbf{B} - \mathbf{M}_\ell||_F^2$ does not increase at each iteration and is bounded below. The above bounded norm sequence does not automatically imply the convergence of $\{\mathbf{A}^t\}$, and $\{\mathbf{B}^t\}$. On the other hand, the proposed method utilizing alternate sequence optimization is a special case of the block coordinate descent algorithm. Both (6) and (7) are Gateaux-differentiable w.r.t. the corresponding variables over its open domain. Using the cyclic rule, each coordinate-wise minimum point of the proposed method is a stationary point according to Theorem 5.1 in [21]. Therefore, the alternating optimization in (6) and (7) produces a sequence of $||\mathbf{A}\mathbf{B} - \mathbf{M}_\ell||_F^2$ that converges to a stationary point.

A. Wavelet Fusion with Hard Thresholding

The wavelet denoising method presented in [6] suggests to decompose the image $\mathbf{M}_\ell$ into subband images through discrete wavelet transform (DWT):

$$\mathbf{M}_\ell \overset{DWT}{\rightarrow} [\ \mathbf{LL}_\ell \quad \mathbf{LH}_\ell \quad \mathbf{HL}_\ell \quad \mathbf{HH}_\ell\ ]. \tag{10}$$

A hard thresholding method is then applied to each component of the high frequency subband coefficients with threshold parameter τ to remove low power noise signal:

$$\begin{aligned}
\mathbf{LH}_\ell[i,j] &= \begin{cases} 0, & |\mathbf{LH}_\ell[i,j]| < \tau, \\ \mathbf{LH}_\ell[i,j], & \text{otherwise;} \end{cases} \\
\mathbf{HL}_\ell[i,j] &= \begin{cases} 0, & |\mathbf{HL}_\ell[i,j]| < \tau, \\ \mathbf{HL}_\ell[i,j], & \text{otherwise;} \end{cases} \\
\mathbf{HH}_\ell[i,j] &= \begin{cases} 0, & |\mathbf{HH}_\ell[i,j]| < \tau, \\ \mathbf{HH}_\ell[i,j], & \text{otherwise,} \end{cases}
\end{aligned}$$

where $0 \leq i \leq (M/2) - 1$, and $0 \leq j \leq (N/2) - 1$ (without lost of generality, we assume the image size of $\mathbf{M}$ is $M \times N$ with even M and N, otherwise an appropriate image border extension technique can be applied). To extend this scheme to multiple images $(\mathbf{M}_1, \ldots, \mathbf{M}_k)$, we propose to fuse the low frequency subband images $\mathbf{LL}_\ell$ as:

$$\mathbf{LL} = \frac{1}{k}\sum_{\ell=1}^{k} \mathbf{LL}_\ell. \tag{11}$$

The high frequency subband images are fused together using the selection of maximum magnitude wavelet coefficients [22] with the hard threshold method such that the wavelet coefficients will be replaced by 0 when the maximum magnitude wavelet coefficients of all the images are smaller than the threshold τ:

$$\begin{aligned}
\mathbf{LH}[i,j] &= \begin{cases} 0, & \text{if } \max_\ell |\mathbf{LH}_\ell[i,j]| < \tau, \\ \mathbf{LH}_\ell[i,j], & \text{otherwise;} \end{cases} \\
\mathbf{HL}[i,j] &= \begin{cases} 0, & \text{if } \max_\ell |\mathbf{HL}_\ell[i,j]| < \tau, \\ \mathbf{HL}_\ell[i,j], & \text{otherwise;} \end{cases} \\
\mathbf{HH}[i,j] &= \begin{cases} 0, & \text{if } \max_\ell |\mathbf{HH}_\ell[i,j]| < \tau, \\ \mathbf{HH}_\ell[i,j], & \text{otherwise.} \end{cases}
\end{aligned} \tag{12}$$

Hence, the denoised image $\hat{\mathbf{X}}$ is obtained by inverse DWT (IDWT) on subband images $[\ \mathbf{LL} \quad \mathbf{LH} \quad \mathbf{HL} \quad \mathbf{HH}\ ]$ as:

$$[\ \mathbf{LL} \quad \mathbf{LH} \quad \mathbf{HL} \quad \mathbf{HH}\ ] \overset{IDWT}{\rightarrow} \hat{\mathbf{X}}. \tag{13}$$

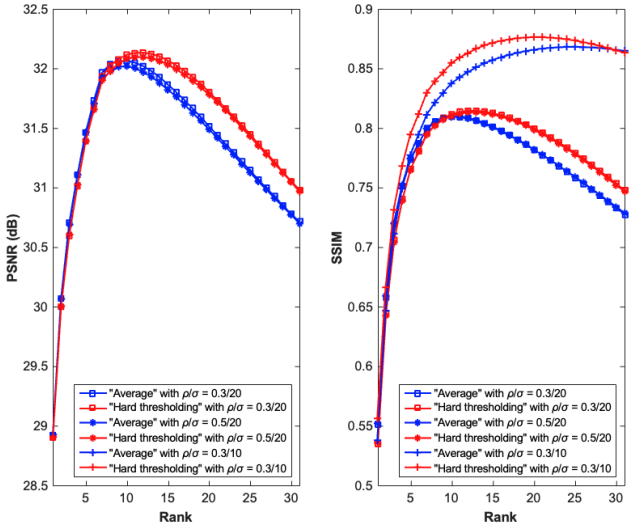

Fig. 1. Effect of different rank r.

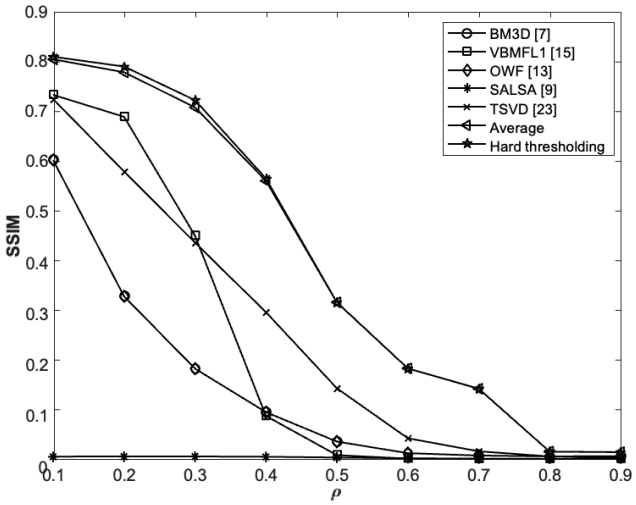

Fig. 2. SSIM versus impulsive noise level.

With an efficient AWGN denoising method, there leaves us the only hurdle is that the generation of the SAPN denoised image set from the noise corrupted image $\mathbf{M}$. We propose to apply a 2-D version of the RIA method to complete the job.

B. 2-D Random Interpolation Averaging

The RIA method has been demonstrated in [11] to handle the AWGN corrupted signal denoising problem very well. However, the extension of the RIA to 2-D RIA is not obvious. Herein, we propose to generate a sequence of sub-image $\mathbf{M}_\ell$ by subsampling with index matrix $\mathbf{\Xi}$, such that:

$$\mathbf{\Xi}_\ell \in \mathbb{R}^{M\times N} \text{with } \mathbf{\Xi}_\ell[i,j] = \{0,1\} \tag{14}$$

and hence the sampled sub-image $\mathbf{M}_\ell$ is given by

$$\mathbf{M}_\ell[i,j] = \begin{cases} \mathbf{M}[i,j], & \text{if } \mathbf{\Xi}_\ell[i,j] = 1, \\ 0, & \text{otherwise.} \end{cases} \tag{15}$$

The elements of the index matrix $\mathbf{\Xi}_\ell[i,j]$ forms a random field. The generation of $\mathbf{\Xi}_\ell[i,j]$ can be roughly classified as i) non-overlap and ii) overlap. Given two distinct and non-null sampling matrices $\mathbf{\Xi}_m$ and $\mathbf{\Xi}_n$ such that $\bigcup_{\ell=1}^{k} \mathbf{\Xi}_\ell$ is a matrix with all elements 1 to span the matrix space. These two sampling matrices do not overlap if and only if $\mathbf{\Xi}_m[i,j] \cdot \mathbf{\Xi}_n[i,j] = 0$ for all $m \neq n$. These two matrices are said to overlap if and only if $\mathbf{\Xi}_m \oplus \mathbf{\Xi}_n \neq 0$, $\mathbf{\Xi}_m[i,j] \cdot \mathbf{\Xi}_n[i,j] \neq 0$ and $(\mathbf{\Xi}_m[i,j] \neq 0) || (\mathbf{\Xi}_n[i,j] \neq 0)$ for $m \neq n$. In this work, the sub-image sequence will contain two non-overlap sub-images $\mathbf{M}_0$ and $\mathbf{M}_1$ and two overlap sub-images $\mathbf{M}_2$ and $\mathbf{M}_3$, such that $\mathbf{M}_0 \bigcup \mathbf{M}_1$ will span $\mathbf{M}$ and $\mathbf{M}_2 \bigcup \mathbf{M}_3$ will also span $\mathbf{M}$. The sampling matrix $\mathbf{\Xi}_0$ is generated with exactly $(M \times N)/2$ elements being 0 and others being 1, where the locations of the 0 valued elements within the sampling matrix are uniformly generated in between $[0, M-1]$ and $[0, N-1]$. Furthermore, $\mathbf{\Xi}_1 = \mathbf{1} - \mathbf{\Xi}_0$ with $\mathbf{1}$ being a matrix with all 1.

On the other hand, before going on with the generation of $\mathbf{\Xi}_2$ and $\mathbf{\Xi}_3$, we need to define three auxiliary non-overlap index matrices $\mathbf{\Omega}_1, \mathbf{\Omega}_2$ and $\mathbf{\Omega}_3$, such that $\sum_{\ell=1}^{3} \mathbf{\Omega}_\ell[i,j] = 1$ and $\mathbf{\Omega}_m \cdot \mathbf{\Omega}_n = 0$ for all $m \neq n$. Suppose that there is η percentage of elements in $\mathbf{\Omega}_1$ being 1, and the non-overlap index matrices $\mathbf{\Omega}_2$ and $\mathbf{\Omega}_3$ have equal elements of 1, where the locations of 1 inside $\mathbf{\Omega}_\ell$ are randomly generated with a uniform distribution. The sampling matrices $\mathbf{\Xi}_2$ and $\mathbf{\Xi}_3$ are generated by the following expressions:

$$\mathbf{\Xi}_2[i,j] = \begin{cases} 1, & \text{if } \mathbf{\Omega}_1[i,j] = 1 \text{ or } \mathbf{\Omega}_2[i,j] = 1, \\ 0, & \text{otherwise,} \end{cases} \tag{16}$$

$$\mathbf{\Xi}_3[i,j] = \begin{cases} 1, & \text{if } \mathbf{\Omega}_1[i,j] = 1 \text{ or } \mathbf{\Omega}_3[i,j] = 1, \\ 0, & \text{otherwise,} \end{cases} \tag{17}$$

respectively. It is vivid that there is η percentage of elements of 1 overlapping in $\mathbf{\Xi}_2$ and $\mathbf{\Xi}_3$. Furthermore, $\mathbf{\Xi}_2 \bigcup \mathbf{\Xi}_3 = \mathbf{1}$ and $\mathbf{\Xi}_2 + \mathbf{\Xi}_3 \neq \mathbf{1}$. As an example, consider $\eta = 50\%$, such that there are $(M \times N)/2$ elements being 1 in $\mathbf{\Omega}_1$, while $\mathbf{\Omega}_2$ and $\mathbf{\Omega}_3$ have $(M \times N)/4$ elements being 1. As a result, the sampling matrices $\mathbf{\Xi}_2$ and $\mathbf{\Xi}_3$ constructed by (16) and (17) will both have 75% elements being 1, while $\mathbf{\Xi}_2$ and $\mathbf{\Xi}_3$ only have 50% of matrix entries of 1 overlaps.

IV. Experimental Results

Simulation results are carried out to demonstrate the denoising performance of the proposed method (denoted as "Hard thresholding") on a real image[3] with large size (960×638), compared with several existing image denoising algorithms,

[3]It is pictured by Machine Nikon D7000 with resolution 4256×2832 and we downloaded from https://pixabay.com/en/bricks-brickwork-wall-dirty-1846866/

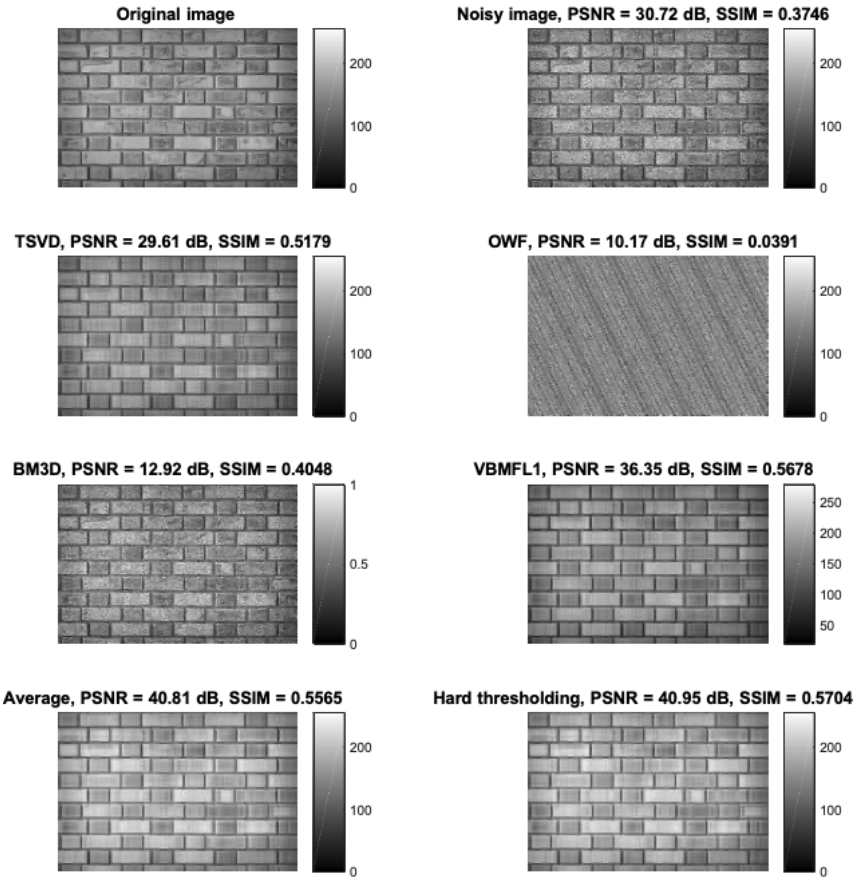

Fig. 3. Performance comparison in mixed noise

i.e., truncated SVD (TSVD) [23], SALSA [9], BM3D [7], OWF [13], VBMFL1 [15].

In Fig. 1, the effect of rank rr on the denoising performance in different ratios of mixed noise is investigated in the sampled grids from 11 to 3131 with interval 2. The PSNR and SSIM are considered as the metric to determine the optimal rank, respectively. It is seen that the highest PSNR and SSIM are obtained when rank r=10r = 10, which implies that our methods have achieved the best image denoising performance at r=10r = 10.

Fig. 2 plots the curves of SSIM versus the SAPN level in the mixed noise. For the comparison of SSIM, we observe that the "Hard thresholding" method yields the best performance on denoising a building image with the SAPN to AWGN ratio ranging from 0.1 to 0.9, where the standard deviation of AWGN is fixed at $\sigma = 20$.

Simulation result on a real image with a large size is implemented in Fig. 3. The normalized noise intensity ρ of SPAN is $\rho = 0.3$ and the hard thresholding parameter is $\tau = 15$. TSVD, BM3D, and OWF are not robust to the mixed noise for restoring the ground truth image with large size, while VBMFL1 and our methods have better denoising performance. Compared with the VBMFL1, the proposed methods enjoy comparable performance in terms of SSIM, and higher PSNR.

V. Conclusion

In this work, a new and effective denoising approach has been developed to preserve the spatial image structure based on the basic LRMF framework. 2-D RIA has been taken advantage under the benefit of randomly generated sub-image sequence, including non-overlap and overlap sub-images. What is more, the mean filtering effect of the image fusion process via a hard threshold wavelet denoising method is developed. The superior performance of the proposed approach is validated by extensive simulation results.

Acknowledgment

We sincerely appreciate Dr. W-S. Tam, Dr. C-W. Kok from Canaan Semiconductor Limited, Hong Kong, and Prof. H.C. So from the City University of Hong Kong, for improving the quality of our work, and the English usage.

This work was supported in part by the National Natural Science Foundation of China under Grant 62202174, in part by the Fundamental Research Funds for the Central

Universities under Grant 2023ZYGXZR085, in part by the Basic and Applied Basic Research Foundation of Guangzhou under Grant 2023A04J1674, and in part by the Guangdong Provincial Key Laboratory of Human Digital Twin under Grant 2022B1212010004.

REFERENCES

[1] S. M. M. Rahman, M. O. Ahmad, and M. N. S. Swamy, "Video denoising based on inter-frame statistical modeling of wavelet coefficients," *IEEE Trans. Circuit Syst. Video Technol.*, vol. 17, no. 2, pp. 187–198, Feb. 2007.

[2] K. Cao, E. Liu, and A. K. Jain, "Segmentation and enhancement of latent fingerprints: A coarse to fine ridgestructure dictionary," *IEEE Trans. Pattern Anal. Mach. Intell.*, vol. 36, no. 9, pp. 1847–1859, Sep. 2014.

[3] Q. Liu, X. Li, and J. Yang, "Optimum co-design for image denoising between type-2 fuzzy identifier and matrix completion denoiser," *IEEE Transactions on Fuzzy Systems*, pp. 1–1, 2020.

[4] A. Buades, B. Coll, and J. Morel, "A review of image denoising algorithms, with a new one," *Multiscale Model. Simul.*, vol. 4, no. 2, pp. 490–530, 2005.

[5] M. Kivanc Mihcak, I. Kozintsev, K. Ramchandran, and P. Moulin, "Low-complexity image denoising based on statistical modeling of wavelet coefficients," *IEEE Signal Process. Lett.*, vol. 6, no. 12, pp. 300–303, Dec. 1999.

[6] D. L. Donoho, "Denoising via soft thresholding," *IEEE Trans. Inf. Theory*, vol. 41, pp. 613–627, May 1995.

[7] K. Dabov, A. Foi, V. Katkovnik, and K. Egiazarian, "Image denoising with block-matching and 3d filtering," in *Electronic Imaging' 06, Proc. SPIE 6064***6064**, no. 6064A-30, 2006, San Jose, California USA.

[8] P. Chatterjee and P. Milanfar, "Patch-based near-optimal image denoising," *IEEE Trans. Image Process.*, vol. 21, no. 4, pp. 1635–1649, Apr. 2012.

[9] M. V. Afonso, J. M. Bioucas-Dias, and M. A. T. Figueiredo, "Fast image recovery using variable splitting and constrained optimization," *IEEE Trans. Image Process.*, vol. 19, no. 9, pp. 2345–2356, Sep. 2010.

[10] W. Dong, X. Li, L. Zhang, and G. Shi, "Sparsity-based image denoising via dictionary learning and structural clustering," in *Proc. IEEE Conf. Comput. Vis. Pattern Recognit. (CVPR)*, Jun. 2011, pp. 457–464, colorado Springs, CO, USA.

[11] Y. Yang and Y. Wei, "Random interpolation average for signal denoising," *IET Signal Process.*, vol. 4, no. 6, pp. 708–719, Dec. 2010.

[12] C. Tomasi and R. Manduchi, "Bilateral filtering for gray and color images," in *Proc. IEEE Conf. Comput. Vis.*, Bombay, India, Jan. 1998, pp. 839–846.

[13] Q. Jin, I. Grama, C. Kervrann, and Q. Liu, "Nonlocal means and optimal weights for noise removal," *SIAM J. Imag. Sci.*, vol. 10, no. 4, pp. 1878–1920, 2017.

[14] S. Gu, L. Zhang, W. Zuo, and X. Feng, "Weighted nuclear norm minimization with application to image denoising," in *Proc. IEEE Conf. Comput. Vis. and Pattern Recognit.*, Columbus, OH, USA, Jun. 2014, pp. 2862–2869.

[15] Q. Zhao, D. Meng, Z. Xu, W. Zuo, and Y. Yan, "L_1 -norm low-rank matrix factorization by variational Bayesian method," *IEEE Trans. Neural Netw. Learn. Syst.*, vol. 26, no. 4, pp. 825–839, Apr. 2015.

[16] J. Cai and R. H. Chan, "Two-phase approach for deblurring images corrupted by impulse plus gaussian noise," *Inverse Problem Imaging*, vol. 2, no. 2, pp. 187–204, 2008.

[17] J. Cai, R. H. Chan, and M. Nikolova, "Fast two-phase image deblurring under impulse noise," *J. Math. Imaging Vis.*, vol. 36, no. 1, p. 46, Aug. 2009.

[18] X. Zhou, C. Yang, H. Zhao, and W. Yu, "Low-rank modeling and its applications in image analysis," *ACM Computing Surveys (CSUR)*, vol. 47, pp. 1 – 33, 2014.

[19] P. Jain, P. Netrapalli, and S. Sanghavi, "Low-rank matrix completion using alternating minimization," in *Proc. ACM Symp. Theory Comput.*, ser. STOC '13. New York, NY, USA: ACM, 2013, pp. 665–674.

[20] D. Gamarnik and S. Misra, "A note on alternating minimization algorithm for the matrix completion problem," *IEEE Signal Process. Lett.*, vol. 23, no. 10, pp. 1340–1343, Oct. 2016.

[21] P. Tseng, "Convergence of a block coordinate descent method for nondifferentiable minimization," *J. Optim. Theory Appl.*, vol. 109, no. 3, pp. 475–494, Jun. 2001.

[22] H. Li, B. S. Manjunath, and S. K. Mitra, "Multisensor image fusion using the wavelet transform," in *Proc. IEEE Conf. image Process.*, 1994, pp. 51–55, Auston, TX, USA.

[23] M. D. Ali, *"Introduction to Inverse Problems in Imaging and Vision"*. Wiley-Blackwell, 2013, ch. 1, pp. 15–58.